Peaking in SS Nuclear Parameters at a Water Interface

T.D. Bohm, M.E. Sawan, B. Smith, P.P.H. Wilson

December 2009

UWFDM-1376

FUSION TECHNOLOGY INSTITUTE

UNIVERSITY OF WISCONSIN

MADISON WISCONSIN

Peaking in SS Nuclear Parameters at a Water Interface

T.D. Bohm, M.E. Sawan, B. Smith, P.P.H. Wilson

Fusion Technology Institute
University of Wisconsin
1500 Engineering Drive
Madison, WI 53706

http://fti.neep.wisc.edu

December 2009

UWFDM-1376

Abstract

The high fidelity high-resolution results for nuclear parameters in ITER FWS modules revealed important heterogeneity effects. Significant peaking in steel nuclear heating occurs at the interface with water because of increased gamma generation in the SS adjacent to the water. This is due to the softer neutron spectrum in the adjacent SS resulting in more gamma generation. Helium production in steel immediately adjacent to the water is larger than the average He production in the steel. This helium production peaking is due to a softer neutron spectrum resulting in increased He production in B-10 and Ni in the SS316LN-IG used in ITER.

1. Introduction

The ITER first wall/shield (FWS) modules consist of a plasma facing first wall (FW) section followed by a shielding section [1]. These modules provide the main thermal and nuclear shielding for the vacuum vessel (VV) and external machine components. The FWS is segmented both in the poloidal and toroidal directions. Eighteen modules with different dimensions are arranged in the poloidal direction with the lowest inboard module designated as Module 1 and the lowest outboard module designated as Module 18. The module toroidal width varies from 1.25 to 1.98 m with the poloidal length varying from 0.85 to 1.24 m. The US is responsible for the design and procurement of modules 7, 12, and 13. The FW panel assembly consists of Be armor, Cu heat sink, and steel structure with embedded water coolant tubes. The shield module is made of steel and is cooled by water. Fig. 1 shows the elements of a design option of the FWS module.

The design process for the FWS modules includes assessment of the stresses due to nuclear heating and performing detailed computational fluid dynamics (CFD) and electromagnetic (EM) analyses. Accurate calculation of the temperature distribution in the FWS module requires accurate knowledge of the plasma heating of the FW and the volumetric nuclear heating due to neutrons and secondary gamma photons. In addition, re-welding is required at several locations in the FWS module and the VV behind it. This requires accurate determination of helium production in the structural material. Therefore, detailed mapping of nuclear heating, radiation damage, and helium production is an essential input to the design process. In previous work [2], we presented the results of the neutronics analysis performed for the conceptual design of Module 13 shown in Fig. 1. We used the Direct Accelerated Geometry MCNP (DAG-MCNP) code [3] developed at the University of Wisconsin. In this code, the neutronics calculations are performed directly in the CAD solid model that allows preserving the geometrical details without any simplification and eliminates possible human error in modeling the geometry. The high fidelity, high-resolution results of the calculations revealed important heterogeneity effects on nuclear parameters. While nuclear heating is higher in steel than in water regions, the steel nearest the water sees the highest nuclear heating. In addition, helium production in the steel immediately adjacent to the water is larger than the average He production in the steel [2]. In this report, the results of this previous analysis are summarized and additional analysis is presented for a simplified geometry to further understand the reasons behind the observed peaking in steel nuclear parameters at the interface with the water coolant.

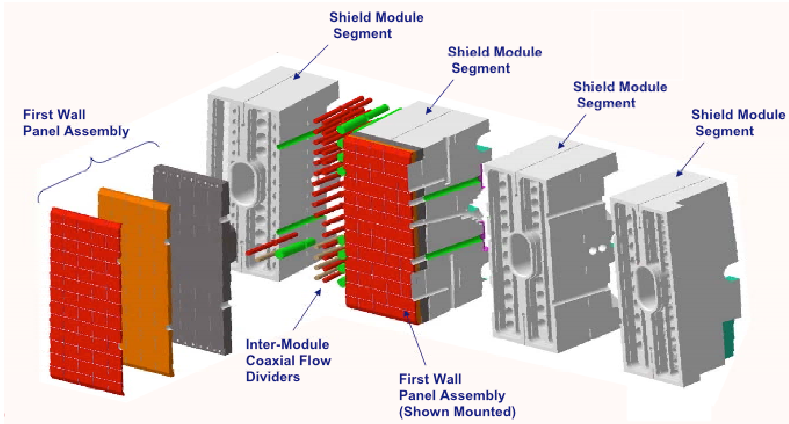

Fig. 1. Elements of the FWS module.

2. Detailed distribution of nuclear parameters in ITER FWS Module 13

In order to capture the impacts of the significant heterogeneity of the FWS module shown in Fig. 1, a hybrid 1-D/3-D neutronics analysis was performed for Module 13. Fundamentally, this model places the 3-D representation of Module 13 into a 1-D model to approximate the coupling to the full machine. In this model, shown in Fig. 2, homogenized radial regions are included to represent the inboard FWS and outboard VV. The extents of the model in the azimuthal and vertical directions are only large enough to accommodate the Module 13 geometry. Reflecting boundary conditions approximate the full extent of ITER in the poloidal and toroidal directions. A 14.1 MeV uniform source between the inboard and outboard sides is used to simulate the ITER plasma. The results were normalized to the neutron wall loading of 0.693 MW/m^2 obtained from 3-D calculations for the full ITER chamber with the exact source distribution [4].

Mesh tallies were used to provide high fidelity 3-D heating, radiation damage, and helium generation profiles through Module 13. These nuclear responses were calculated on 0.5 cm x 0.5 cm x 1 cm mesh elements. Fig. 3 shows all three responses calculated on a cylindrical surface 11.5 cm from the front of the FW (within the front reservoir), with 17 million source particles sampled. While the nuclear heating results are represented for the actual material existing at each location, the He production and radiation damage results represent the nuclear response to stainless steel when placed in the neutron flux at each point even in the water zone. The cumulative end-of-life parameters were determined for the ITER average FW fluence goal of 0.3 MWa/m^2. Mesh-based weight windows were used for variance reduction leading to statistical uncertainties <5%. Additional visualizations of the results have been developed to permit a more integrated view of the variations. Fig. 4 provides a visualization of the nuclear heating throughout the front part of the FWS. It clearly shows the variation of nuclear heating due to geometrical changes and attenuation as one moves from the front of the FW deeper into the FWS module.

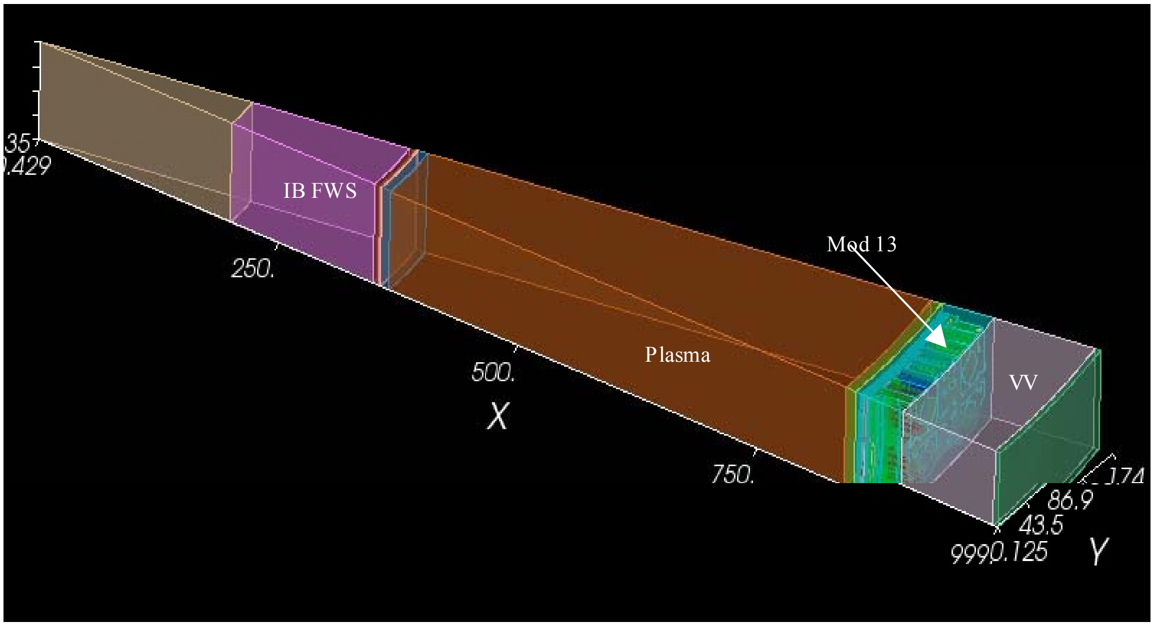

Fig. 2. Hybrid 1-D/3-D model.

Significant variations in heating and He production occur at each radial location as a result of heterogeneity while much less variation is observed in atomic displacement damage. In addition, these high fidelity, high-resolution results reveal important heterogeneity effects on nuclear parameters. While at a given radial location, nuclear heating is higher in steel than in water regions, the steel nuclear heating peaks at the interface with water. While the He production results inside the water reservoir itself are not physically meaningful, they do indicate that the softened neutron energy spectrum in the water regions would lead to a higher He production in steel and thus suggests that He production in the steel immediately adjacent to the water is larger than the average He production in the steel with possible implications on reweldability.

3. Assessment of peaking in SS nuclear heating at interface with water

In order to fully understand the source of the peaking in nuclear parameters at the SS/water interface, we performed additional calculations on a generic model. Both MCNP [5] and DANTSYS [6] calculations were performed for a system consisting of a 30 cm thick SS slab followed by a 30 cm thick water slab. 14 MeV neutrons are incident on the front surface of the SS zone. We used the detailed elemental composition of the materials of the FWS modules as provided by the ITER international organization (IO) [7]. The compositions used for SS and water are given in Table 1.

Fig. 5 compares the neutron energy spectra at the front of the SS zone, near the interface between the SS and water, and at the back of the water zone. It is clear that significant spectrum softening occurs in the SS zone as one moves from the front to the back at the interface with the water zone. The number of neutrons in the lowest energy bin (0-0.25 MeV) at the SS interface with water is a factor of 1.65 higher than at the front surface of SS. This is attributed to the enhanced neutron slowing down in the adjacent water. More spectrum softening occurs as one moves deeper in the water slab due to the significant neutron slowing down in water.

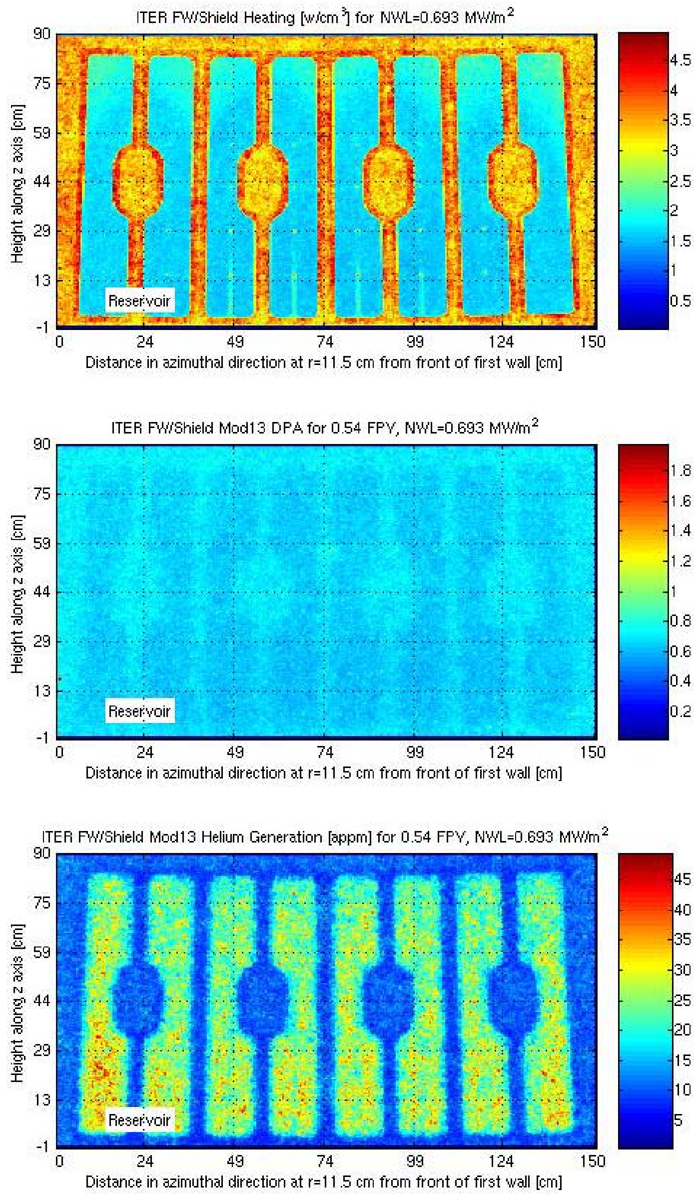

Fig. 3. Nuclear responses (nuclear heating, radiation damage, He production) in Module 13 at a distance of 11.5 cm from the front of the first wall.

Figs. 6 and 7 show the spatial variation of the total neutron and gamma fluxes as a function of depth in the SS and water zones obtained from the MCNP and DANTSYS calculations, respectively. It is clear that while the neutron flux continues to decrease as one moves from the SS zone to the water zone, the gamma flux increases as we approach the interface with water in the SS zone and stays at a relatively high value in the water zone. This results from the large gamma generation in water and the larger gamma generation in SS at the vicinity of the water interface resulting from the softer neutron spectrum. The significant neutron spectrum softening as one moves from the steel to the water is clearly demonstrated in Fig. 7.

Table 1. Material composition used for SS and water.

SS316LN-IG (220°C)

Element	**Atom Density (atom/b.cm)**
c	8.8989E-05
mn55	1.5718E-03
ni	1.0017E-02
cr	1.6149E-02
mo	1.2510E-03
n14	2.3893E-04
p31	3.8721E-05
s	1.1221E-05
si	8.5422E-04
nb93	5.1637E-06
ta181	2.6509E-06
ti	1.5033E-04
cu	7.5511E-05
co59	4.0702E-05
b10	9.5345E-07
b11	3.4904E-06
al27	8.8901E-05
o16	5.9841E-06
k	6.1345E-07
bi209	1.8365E-07
v	3.7668E-06
zr	1.0517E-06
sn	8.0826E-07
w	2.6065E-07
pb	1.8258E-07
fe	5.5790E-02
Total	8.6391E-02

Water (125°C,3MPa)

Element	**Atom Density (atom/b.cm)**
h1	6.3656E-02
h2	9.5499E-06
o16	3.1756E-02
total	9.5422E-02

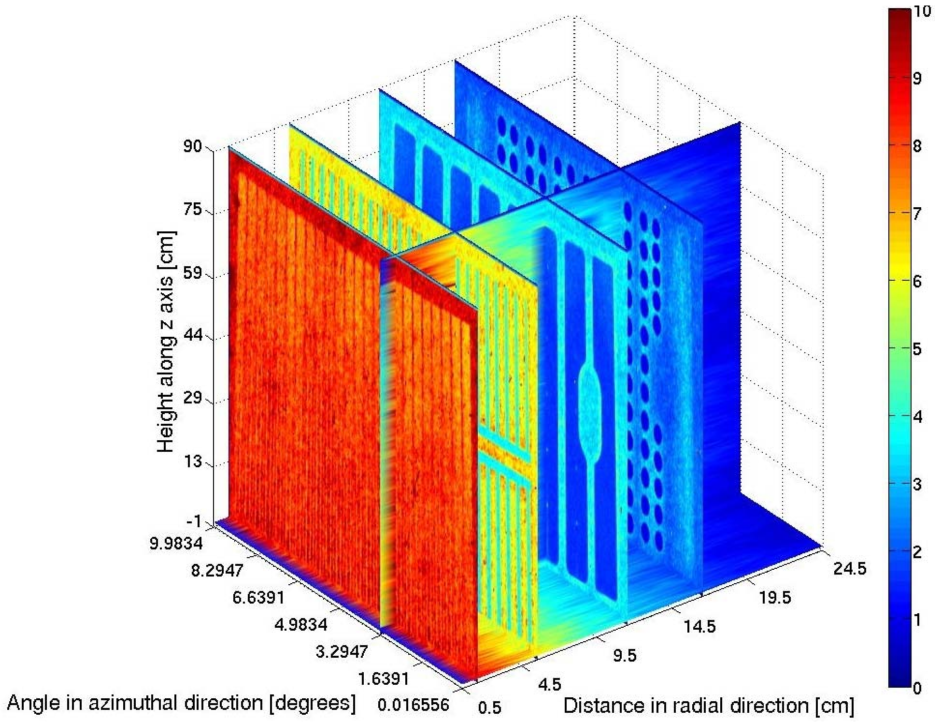

Fig. 4. 3-D visualization of nuclear heating in FWS module.

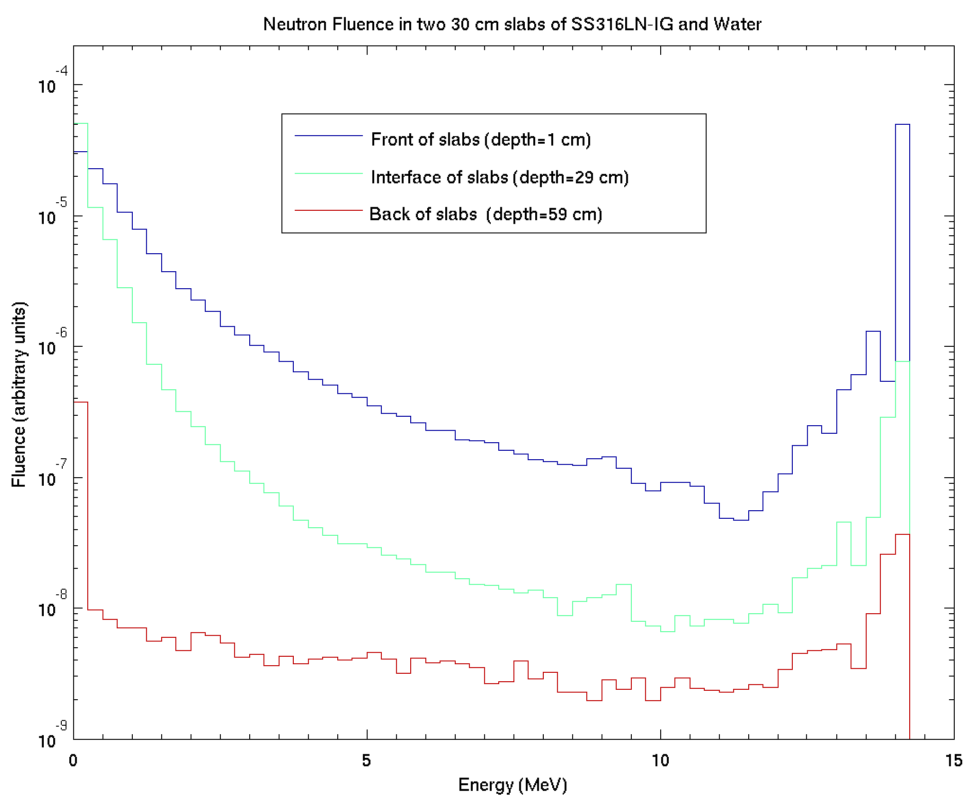

Fig. 5. Neutron fluence at three different depths in a slab consisting of 30 cm of SS316LN-IG and 30 cm of water.

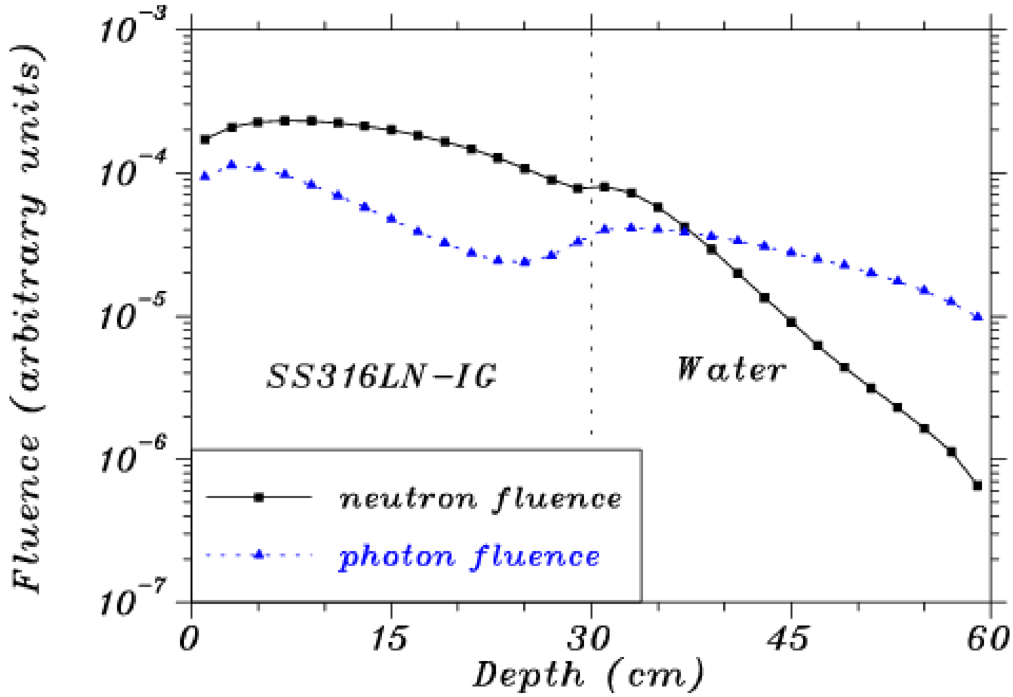

Fig. 6. Total neutron and photon fluence versus depth from MCNP calculations.

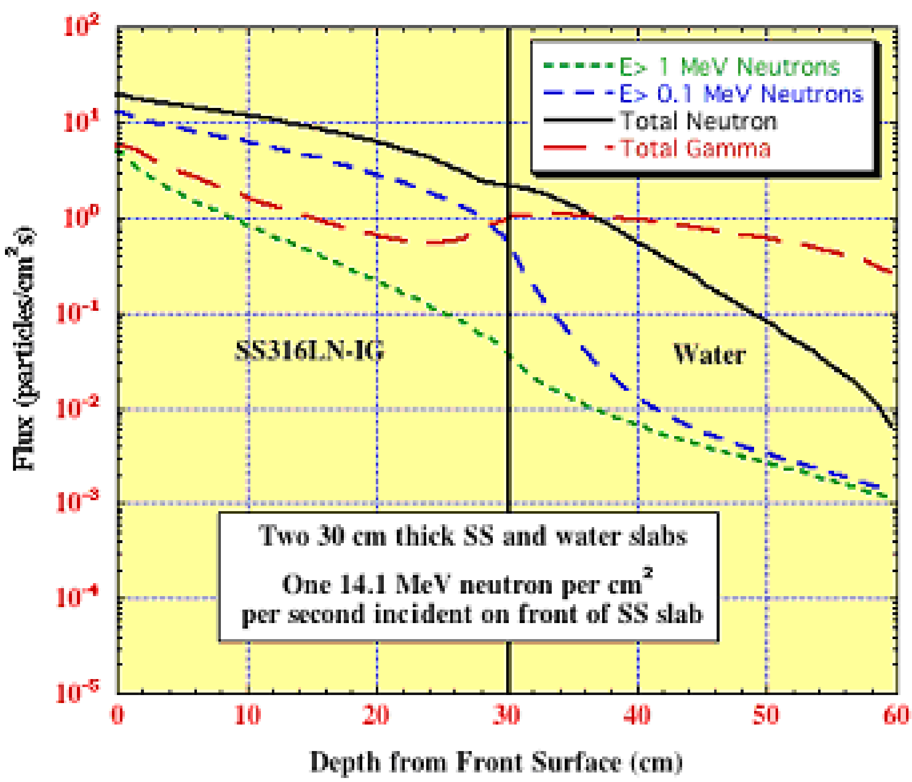

Fig. 7. Neutron and photon fluxes versus depth from DANTSYS calculations.

Figs. 8 and 9 give the spatial variation of nuclear heating as a function of depth from MCNP and DANTSYS calculations, respectively. Both the neutron and gamma heating results are shown in addition to the total nuclear heating. Neutron heating in SS decreases as one moves from the surface facing the neutron source towards the interface with water. On the other hand, gamma heating (which dominates nuclear heating in SS) begins to increase as one approaches the interface with water. These results reflect the spatial variation in neutron and gamma fluxes shown in Figs. 6 and 7. Fig. 10 shows the amount of gammas produced from neutron interactions at locations in SS and water. It is clear that gamma production is higher on the SS side of the interface than in the water side. It is also clear that there is a sharp peak in photon production per neutron on the SS side of the SS/water interface. This may indicate that the larger gamma heating in SS at the interface is primarily due to the enhanced gamma generation in SS from the softened neutron spectrum in the vicinity of water.

To better understand the peak in photon heating near the interface, additional investigations were carried out with MCNP. The photon heating in the SS cell just before the interface (thickness = 2 cm) was investigated using the cell flagging and tally tagging features of MCNPX. The cell flagging shows that of the histories that contribute to this "tally of interest", more than 90% were in the water at one time (either as neutrons or photons). Fig. 11 shows the result of using the tally tagging feature on this "tally of interest" to indicate the location of the origin of the scoring particle (i.e. the location where the scoring photons originate). This figure shows that most (75%) of the photons that contribute to the "tally of interest" originate from the SS just before the interface. Collectively, this cell flagging and tally tagging information indicates that there are two possible history scenarios for the majority of photons contributing to the tally of interest. One is that neutrons enter the water and are scattered back at lower energy to the last section of SS near the interface. These lower energy neutrons then produce increased numbers of photons that then lead to the peak in photon heating. The other possible scenario is that neutrons produce photons in the last section of SS, they enter the water and are then scattered back into the last section of SS producing the peak in the photon heating. Further investigation performed by setting photon importances to zero in the water indicates that scenario 1 described above is more dominant.

4. Assessment of peaking in SS helium production at interface with water

The spatial variation in the SS helium production is shown in Figs. 12 and 13 from MCNP and DANTSYS calculations, respectively. It shows a significant increase as one approaches the interface with water. Helium is generally produced by high energy neutrons in the main constituent elements of SS and the softer energy spectrum at the interface is not expected to result in increased He production. We investigated the impact of removing minor constituent elements and impurities on He production. The effect was very small except for the removal of boron. Removing the 10 wppm B from the SS316LN-IG resulted in significant reduction in He production at the interface as shown in Figs. 12 and 13. Hence, the peaking in He production at the interface is due to the enhanced He production from B-10. The large (n,α) cross section of B-10 at low energies combined with the much softer neutron energy spectrum causes the significant increase in He production. A similar but smaller effect is observed for atomic displacement damage, as shown in Fig. 14, due to increased damage energy from the recoil nuclides following

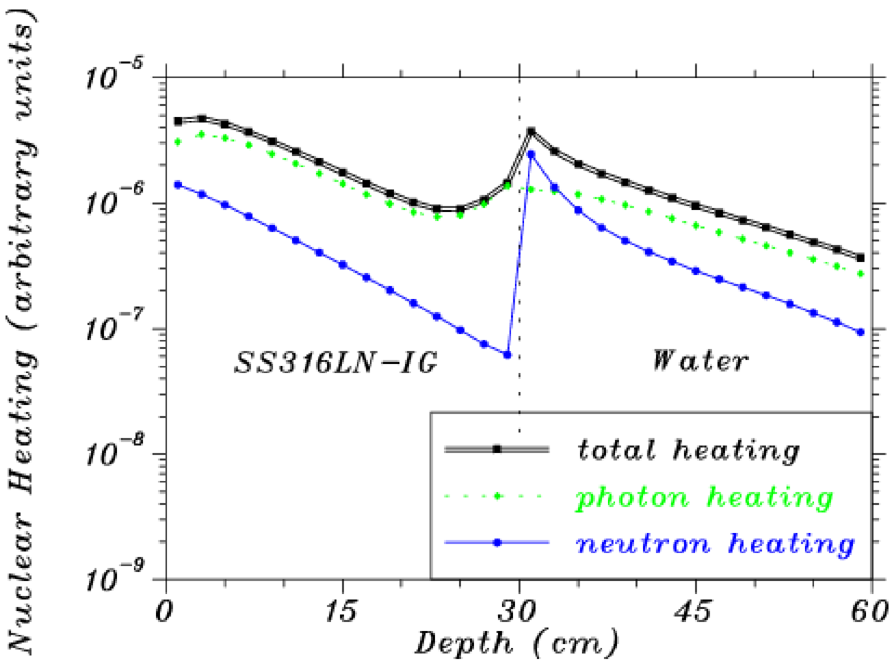

Fig. 8. Nuclear heating versus depth from MCNP calculations.

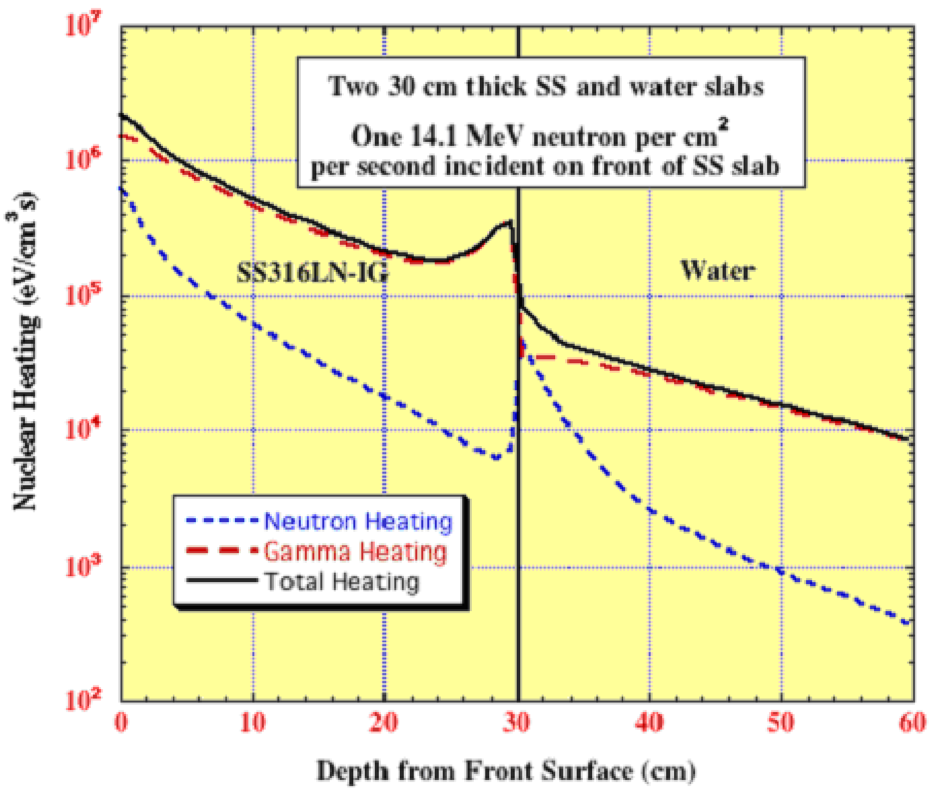

Fig. 9. Nuclear heating versus depth from DANTSYS calculations.

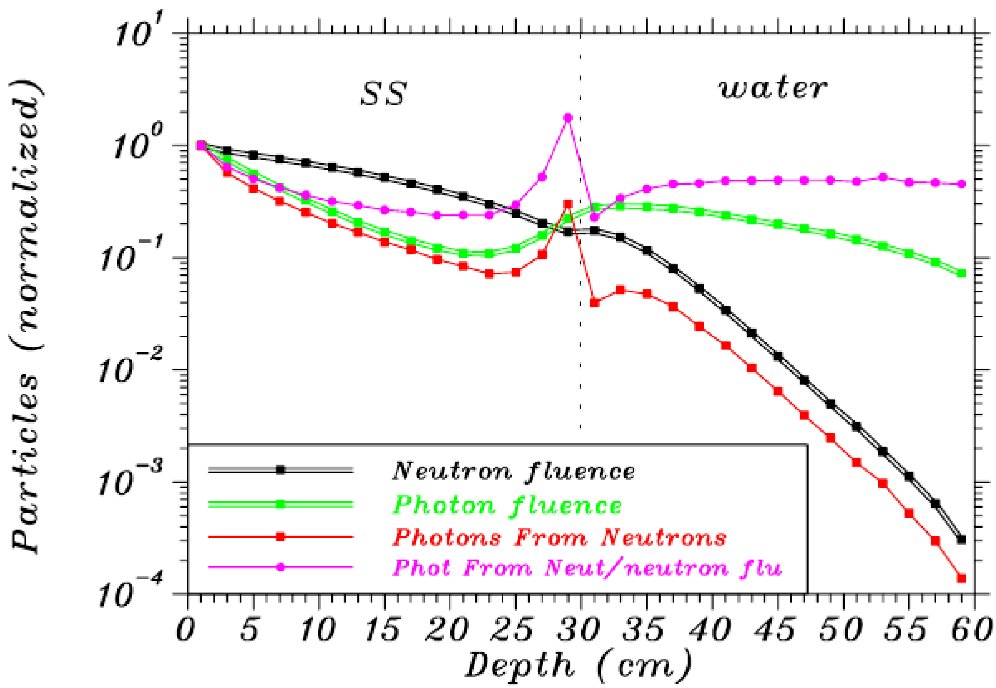

Fig. 10. Spatial variation of gamma photon production from neutrons.

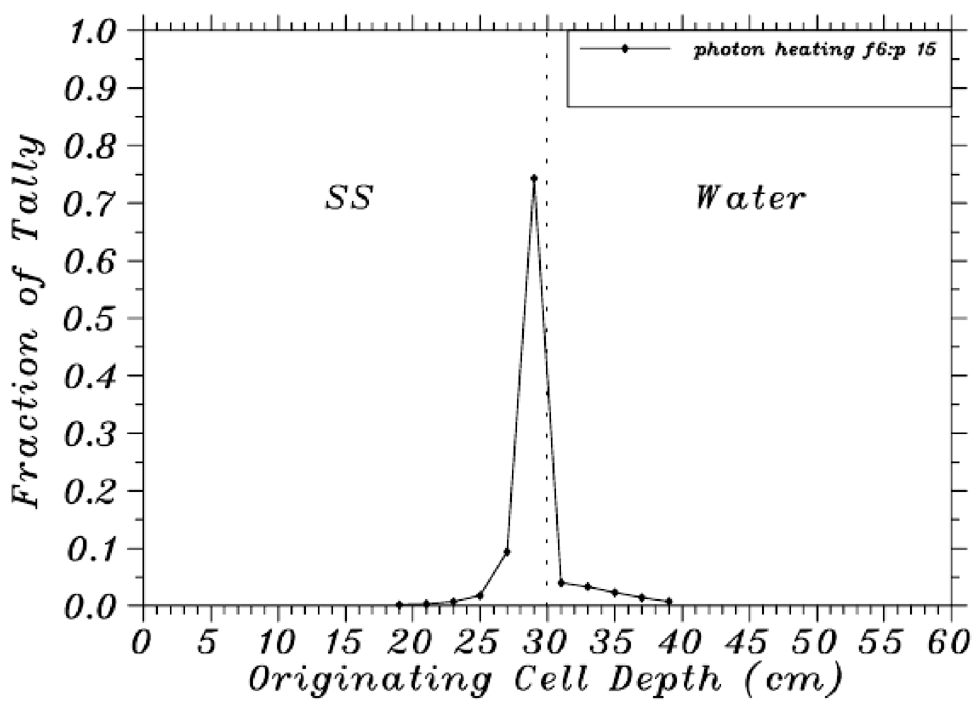

Fig. 11. Location of origin of scoring particles for “tally of interest”.

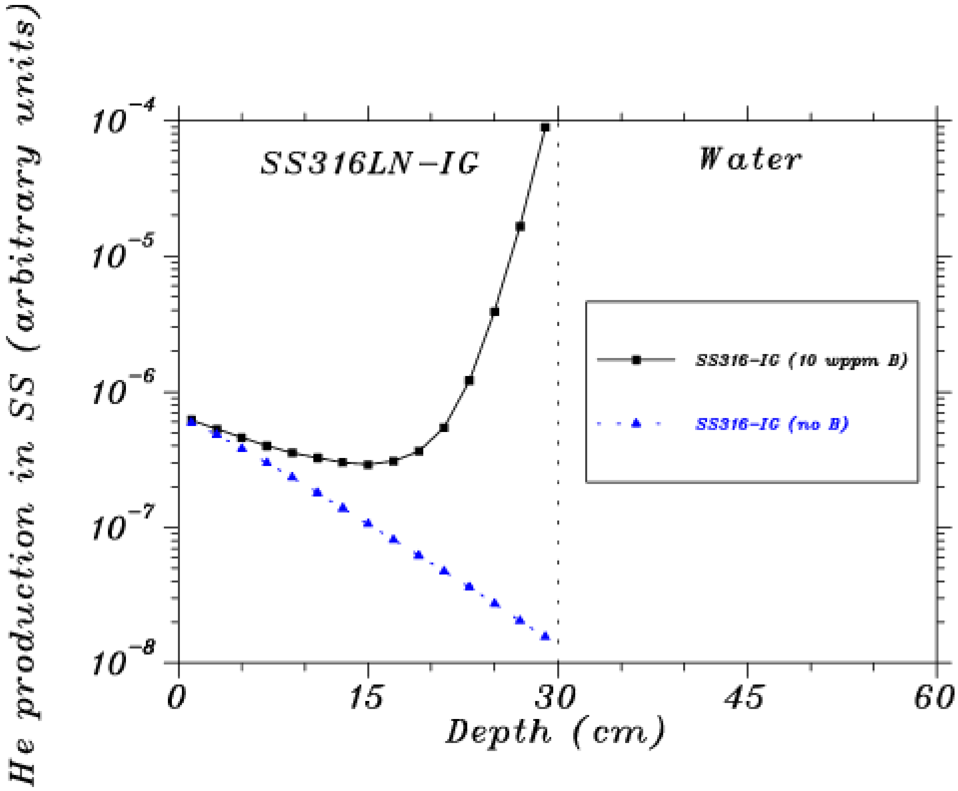

Fig. 12. He production in SS316 versus depth from MCNP calculations.

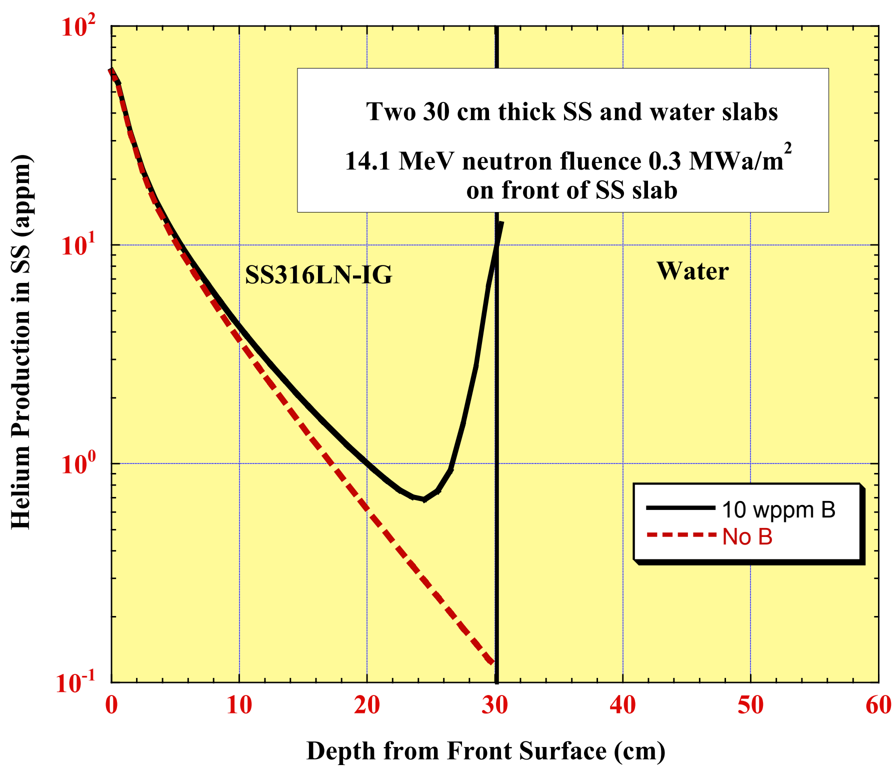

Fig. 13. He production in SS316 versus depth from DANTSYS calculations.

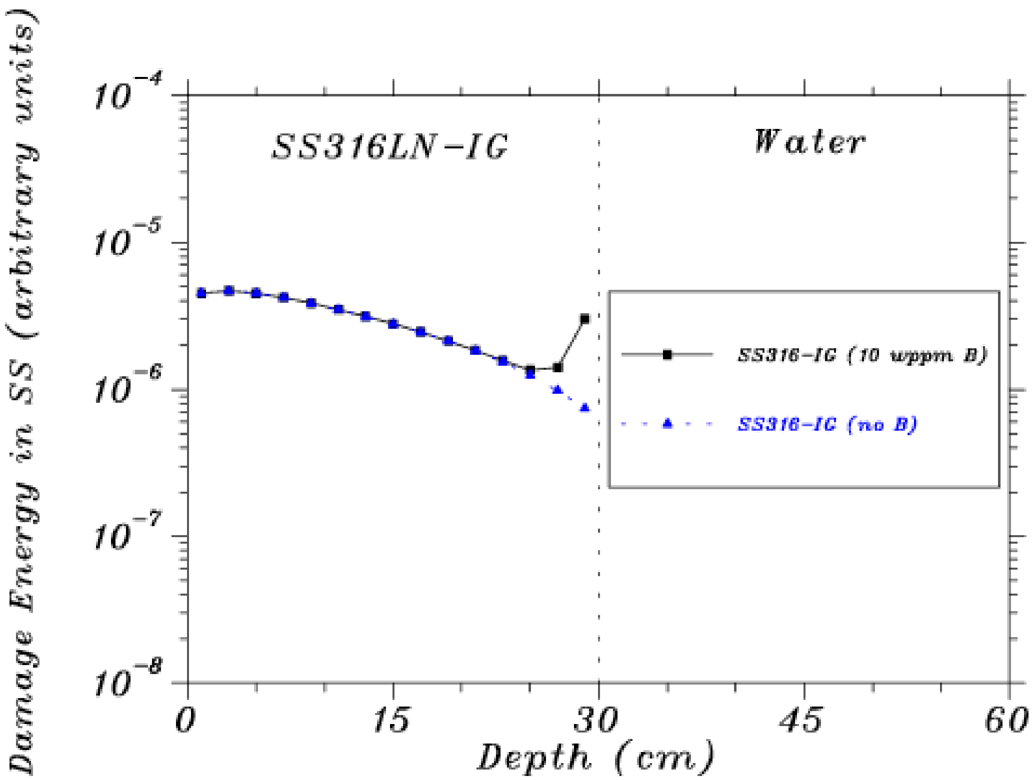

Fig. 14. Total damage energy in SS316 versus depth.

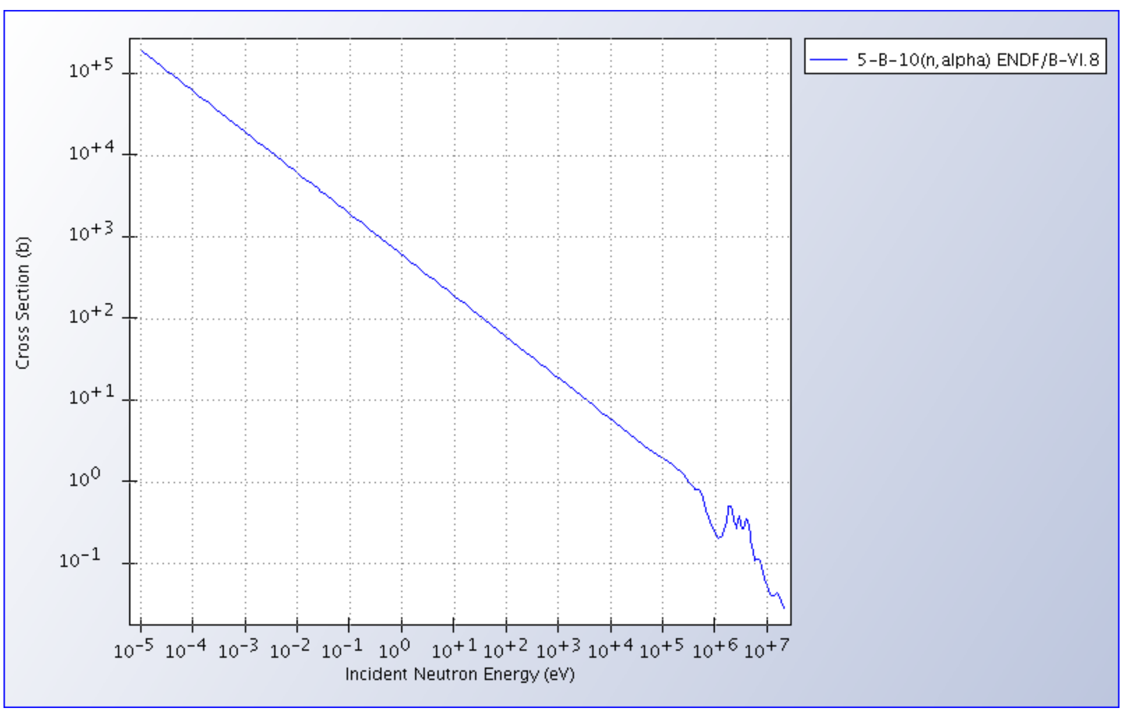

Fig. 15. B-10 (n,α) cross section.

the B-10 (n,α) reaction. The B-10(n,α) cross section used in FENDL-2.1 data [8] is plotted in Fig. 15.

Another contribution to helium production comes from a two-step $^{58}Ni(n,\gamma)^{59}Ni(n,\alpha)$ reaction of low-energy neutrons with Ni. With 12.25 wt% Ni in the SS used in ITER, this sequential reaction is expected to enhance helium production near the interface with water due to the significant neutron energy spectrum softening. This effect is not included in neutronics calculations with MCNP and DANTSYS where only primary reactions are considered. To investigate this contribution, we performed calculations with the ALARA activation code [9] where the neutron flux determined from the DANTSYS neutronics calculations was used to evaluate secondary isotopes produced and their subsequent nuclear reactions. Fig. 16 gives the spatial variation of helium production determined with ALARA for the cases with and without B. Notice that even if the boron is removed, there is a slight peaking in helium production at the interface due to the enhanced contribution from Ni interacting with the softened neutron spectrum. Fig. 17 compares the results without boron from DANTSYS where the produced isotope Ni-59 is not included and from ALARA where it is included. Comparing the results in Figs. 13 and 16 indicates that the peak value with boron at the interface decreased by 28% when ALARA was used. The ALARA calculations account also for boron depletion that is larger at the interface with water, as shown in Fig. 18, where the neutron spectrum is significantly softer. Nearly half of the boron will be depleted at the interface at a fluence corresponding to the end-of-life of ITER.

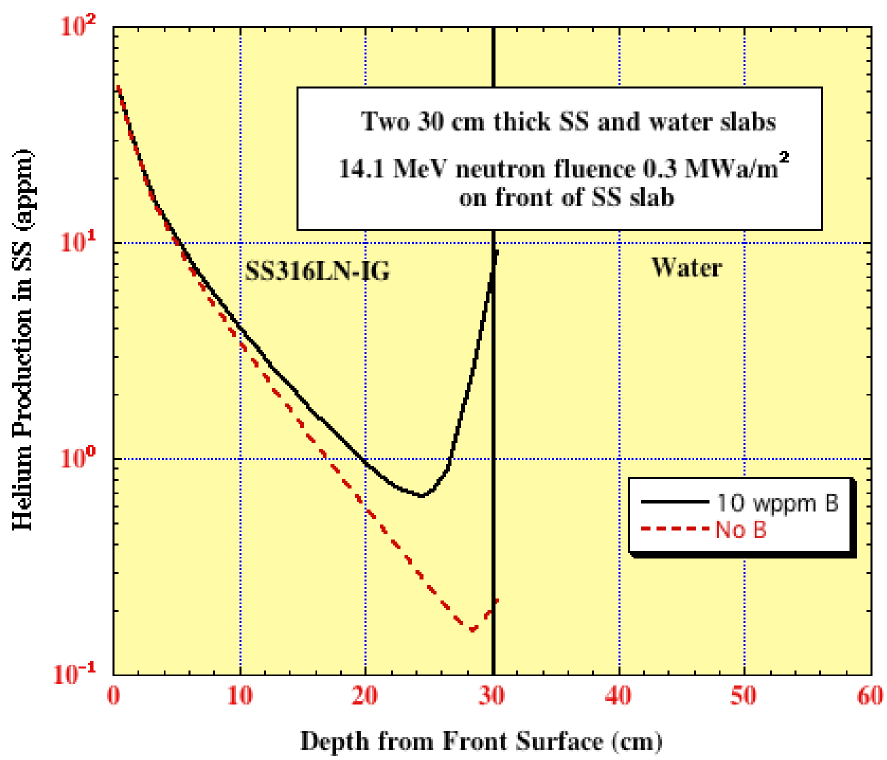

Fig. 16. He production in SS316 versus depth from ALARA calculations with and without B.

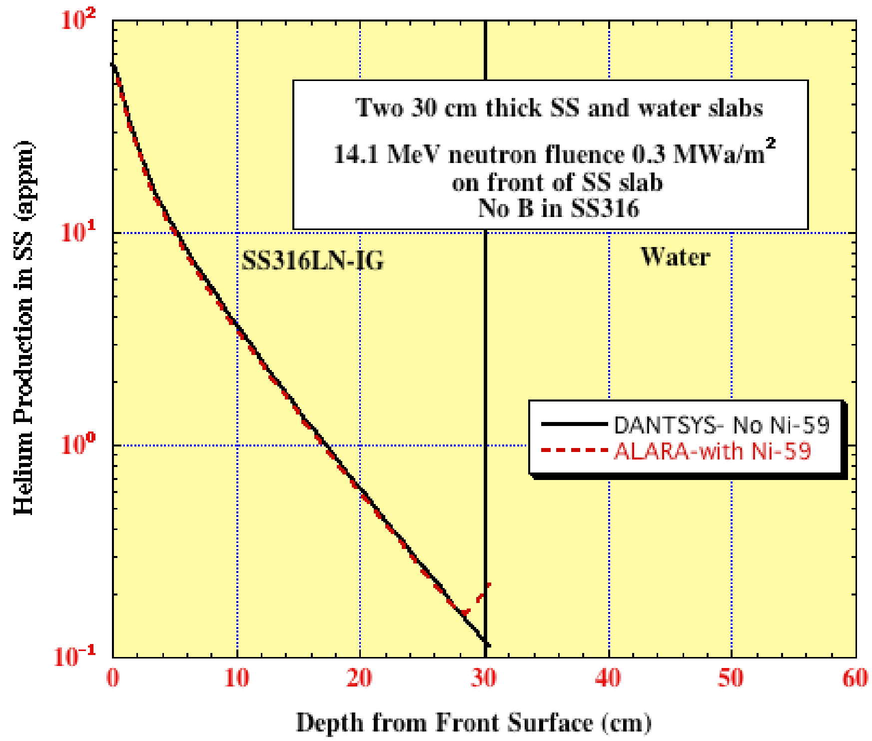

Fig. 17. Contribution of Ni to He production peaking at interface.

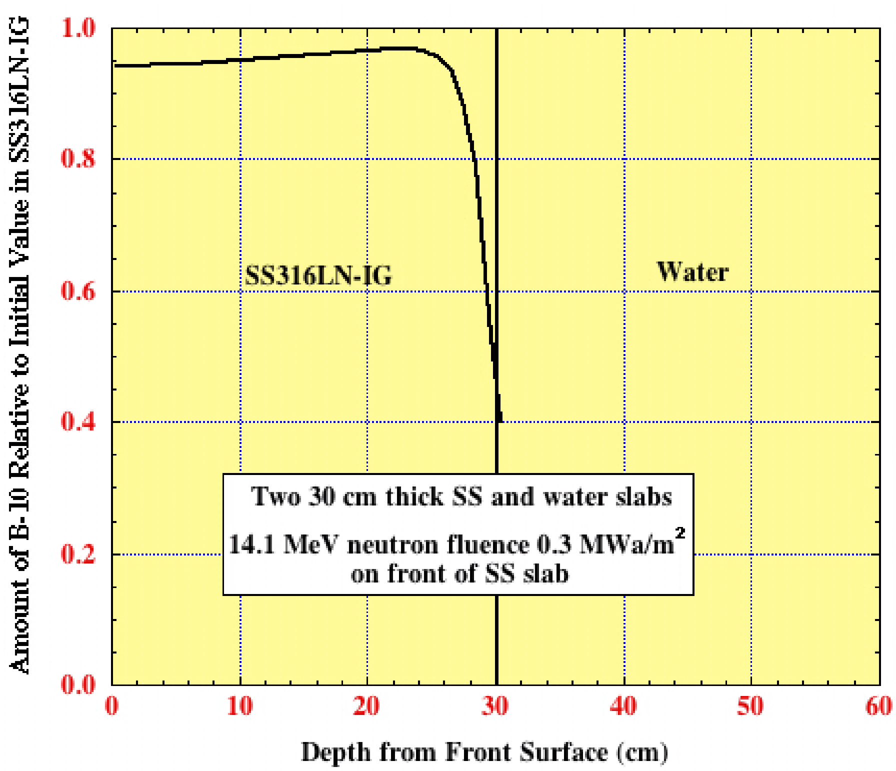

Fig. 18. Spatial variation of boron depletion from ALARA calculations.

5. Conclusions

The high fidelity high-resolution results for nuclear parameters in ITER FWS modules revealed important heterogeneity effects. While at a given radial location in a shield module, nuclear heating is higher in steel than in water regions, the steel nearest the water sees the highest nuclear heating because of the softer neutron spectrum in this portion of the SS resulting in more gamma generation. From an engineering perspective, it is preferable to have the peak heating closer to the heat removal surface, so this effect is ultimately beneficial. Helium production in steel immediately adjacent to the water is larger than the average He production in the steel. Helium production peaking in steel at the interface with water is due to a softer neutron spectrum resulting in increased He production primarily in B-10. Another secondary contribution comes from helium production in a two-step reaction of low-energy neutrons with Ni. The SS316LN-IG used in the ITER FWS has 10 wppm B and 12.25 wt% Ni. This effect is important for re-welding considerations. The local quality of welds could be compromised in the steel immediately adjacent to the coolant. This may be an important consideration in designing the fabrication and maintenance plans for components in the ITER FWS and in fusion energy systems in general.

References

[1] ITER Design Description Document, 1.6 Blanket, ITER Document ITER_D_22F3M6 v2.0, August 2004.

[2] B. Smith, P. Wilson, and M. Sawan, "Three Dimensional Neutronics Analysis of the ITER First Wall/Shield Module 13," Proc. IEEE/NPSS 22nd Symposium on Fusion Engineering, Albuquerque, NM, June 17-21, 2007, IEEE (2007).

[3] T. Tautges, P.P.H. Wilson, J. Kraftcheck, B. Smith, and D. Henderson, "Acceleration Techniques for Direct Use of CAD-Based Geometries in Monte Carlo Radiation Transport," Proceedings of International Conference on Mathematics, Computational Methods & Reactor Physics (M&C 2009), Saratoga Springs, New York, May 3-7, 2009.

[4] P. Wilson, et al., "State of the Art 3-D Radiation Transport Methods for Fusion Energy Systems," Fusion Engineering and Design, vol. 83, pp. 824-833 (2008).

[5] X-5 Monte Carlo Team, "MCNP-A General Monte Carlo N-Particle Transport Code, Version 5-Volume II: Users Guide," LA-CP-03-0245, Los Alamos National Laboratory (April 2003, revised 2/1/2008).

[6] R.E. Alcouffe, R. Baker, F. Brinkley, D. Marr, R. O'Dell, and W. Walters, "DANTSYS 3.0, A Diffusion Accelerated Neutral Particle Transport Code System," LA-12969-M, Los Alamos National Laboratory (June 1995).

[7] Materials Assessment Report, Appendix B-Chemical Composition of Materials, ITER Document ITER_D_22F2PH_v.2, July 2004.

[8] D.L. Aldama and A. Trkov, "FENDL-2.1, Update of an Evaluated Nuclear Data Library for Fusion Applications," Report INDC(NDS)-467, International Atomic Energy Agency (2004).

[9] P.P.H. Wilson, "ALARA: Analytic and Laplacian Adaptive Radioactivity Analysis," Ph.D. Thesis, University of Wisconsin-Madison Fusion Technology Institute UWFDM-1098 (April 1999).